Early onset and late acceleration of rapid exhumation in the Namche Barwa syntaxis, eastern Himalaya

Gwladys Govin, Peter van Der Beek, Yani Najman, Ian Millar, Lorenzo Gemignani, Pascale Huyghe, Guillaume Dupont-Nivet, Matthias Bernet, Chris Mark, Jan Wijbrans

Early onset and late acceleration of rapid exhumation in the Namche Barwa syntaxis, eastern Himalaya

Gwladys Govin[1†], Peter van der Beek[2,3*], Yani Najman[1], Ian Millar[4], Lorenzo Gemignani[5‡], Pascale Huyghe[2], Guillaume Dupont-Nivet[3,6], Matthias Bernet[2], Chris Mark[7§] and Jan Wijbrans[5]

[1]Lancaster Environment Centre, Lancaster University, Lancaster LA1 4YQ, UK
[2]Institut des Sciences de la Terre (ISTerre), Université Grenoble Alpes, 38058 Grenoble, France
[3]Institute of Geosciences, Potsdam University, 14476 Potsdam, Germany
[4]NERC Isotope Geosciences Laboratory (NIGL), British Geological Survey, Keyworth NG12 5GG, UK
[5]Department of Earth Sciences, Vrije Universiteit Amsterdam, 1081 HV, Amsterdam, Netherlands
[6]Géosciences Rennes, CNRS, Université de Rennes 1, 35042 Rennes, France
[7]Department of Geology, Trinity College Dublin, Dublin 2, Ireland

ABSTRACT

The Himalayan syntaxes, characterized by extreme rates of rock exhumation co-located with major trans-orogenic rivers, figure prominently in the debate on tectonic versus erosional forcing of exhumation. Both the mechanism and timing of rapid exhumation of the Namche Barwa massif in the eastern syntaxis remain controversial. It has been argued that coupling between crustal rock advection and surface erosion initiated in the late Miocene (8–10 Ma). Recent studies, in contrast, suggest a Quaternary onset of rapid exhumation linked to a purely tectonic mechanism. We report new multisystem detrital thermochronology data from the most proximal Neogene clastic sediments downstream of Namche Barwa and use a thermo-kinematic model constrained by new and published data to explore its exhumation history. Modeling results show that exhumation accelerated to ~4 km/m.y. at ca. 8 Ma and to ~9 km/m.y. after ca. 2 Ma. This three-stage history reconciles apparently contradictory evidence for early and late onset of rapid exhumation and suggests efficient coupling between tectonics and erosion since the late Miocene. Quaternary acceleration of exhumation is consistent with river-profile evolution and may be linked to a Quaternary river-capture event.

INTRODUCTION

The Nanga Parbat and Namche Barwa massifs, at the respective western and eastern syntaxial terminations of the Himalaya (Fig. 1), share characteristics that have focused research into the coupling between tectonics and surface processes (Zeitler et al., 2001b; Finnegan et al., 2008; Korup et al., 2010; Koons et al., 2013; Wang et al., 2014). Both massifs show young (<10 Ma) high-grade metamorphism and partial melting (Burg et al., 1998; Zeitler et al., 2001a, 2014; Booth et al., 2009), extreme relief, and

rapid erosion (Burbank et al., 1996; Finnegan et al., 2008), expressed by exceptionally young thermochronologic ages (Stewart et al., 2008; Enkelmann et al., 2011; Bracciali et al., 2016; King et al., 2016). The two largest Himalayan rivers, the Indus and the Yarlung-Tsangpo-Siang-Brahmaputra, show hairpin bends and kilometer-scale steepened knickzones as they cross these massifs (Fig. 1), sparking a debate on potential erosional controls on tectonics (Zeitler et al., 2001b; Finnegan et al., 2008; Seward and Burg, 2008; Wang et al., 2014; King et al., 2016).

Several models seek to explain these remarkable features. Purely tectonic mechanisms include range-parallel buckling in the indenter-plate corner (Burg et al., 1998), uplift driven by a geometrically stiffened bend in the subducting plate (Bendick and Ehlers, 2014), and orogen-parallel crustal transport arising from velocity

and/or strain partitioning (Whipp et al., 2014). In contrast, the tectonic-aneurysm model (Zeitler et al., 2001a, 2001b; Koons et al., 2013) calls for coupling between river incision and rapid exhumation, leading to local crustal weakening and focusing rock pathways into the weakened, rapidly eroding zone. The inflowing material promotes topographic relief growth, localized exhumation, and crustal weakening, creating a positive feedback loop between tectonics and surface processes.

Besides the mechanism, the timing of rapid exhumation is also controversial in the Namche Barwa massif. Early bedrock geochronology and thermochronology studies estimated the onset of rapid exhumation at ca. 4 Ma (Burg et al., 1998; Seward and Burg, 2008), whereas more recent data (Booth et al., 2009; Zeitler et al., 2014) have suggested 8–10 Ma. Detrital thermochronology studies from the Brahmaputra Valley, the Surma Basin (Bangladesh), and the offshore Bengal Fan have proposed rapid syntaxial exhumation starting at either 4–6 Ma (Najman et al., 2019) or <3 Ma (Chirouze et al., 2013; Bracciali et al., 2016). This inconsistency may arise from downstream modification and dilution of characteristic syntaxial exhumation signals (Bracciali et al., 2016; Gemignani et al., 2018); the most robust signal is therefore expected in proximal sedimentary records. Lang et al. (2016) modeled detrital thermochronology data from the proximal Siji section (Fig. 1) to infer an onset of rapid exhumation in Namche Barwa at 5–7 Ma.

To explore the exhumation history of the Namche Barwa massif in more detail, we present new multisystem detrital thermochronology

[†]Deceased.
[*]E-mail: vanderbeek@uni-potsdam.de
[‡]Current address: Institute of Geological Sciences, Freie Universität Berlin, 12249 Berlin, Germany.
[§]Current address: School of Earth Sciences, University College Dublin, Dublin D04 V1W8, Ireland.
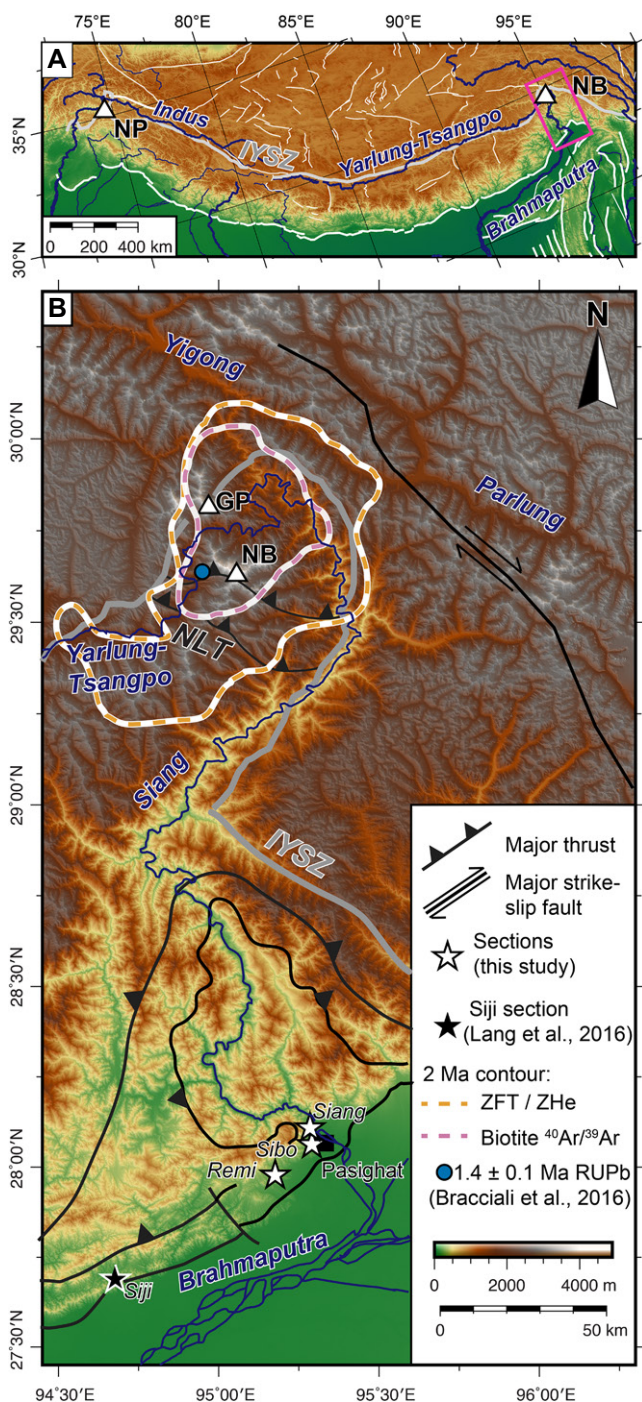
Figure 1. (A) Topography, active faults (white), and major rivers (blue) of the Himalaya. Triangles show syntaxial massifs: NP—Nanga Parbat; NB—Namche Barwa. Box shows location of panel B. IYSZ—Indus-Yarlung suture zone. (B) Eastern syntaxis, showing Namche Barwa massif, Yigong, Parlung, and Yarlung-Tsangpo-Siang-Brahmaputra Rivers, and sampling locations. Stars indicate sampled sections; black lines show major faults. Orange and purple dashed lines are contours of zircon fission-track–zircon (U-Th)/He (ZFT/ZHe) and biotite $^{40}Ar/^{39}Ar$ cooling ages <2 Ma, respectively (Gemignani et al., 2018). NB—Namche Barwa; GP—Gyala Peri; NLT—Nam La thrust; RUPb—rutile U-Pb age.

data from Neogene foreland-basin samples collected directly downstream of the syntaxis (Fig. 1) and interpret these using a thermo-kinematic inverse model.

NEW DETRITAL THERMOCHRONOLOGY DATA

We collected ten sandstone samples from three sedimentary sections close to the Siang-Brahmaputra confluence (Fig. 1). These sections are described by Govin et al. (2018), who also determined depositional ages ranging from 0.5 ± 0.3 Ma to 10.0 ± 2.0 Ma (see Table S1 in

the Supplemental Material[1]). Provenance data indicate that the source region for these deposits included the Namche Barwa massif (Govin et al., 2018). Here we present new zircon fission-track (ZFT), muscovite $^{40}Ar/^{39}Ar$ (MAr), and rutile U-Pb (RUPb) data. Closure temperatures of these thermochronometers range from ~300 °C

[1]Supplemental Material. Methods descriptions, analytical data, and inversion results. Please visit https://doi.org/10.1130/GEOL.S.12620630 to access the supplemental material, and contact editing@geosociety.org with any questions.

(ZFT) to >500 °C (RUPb), depending on grain size, composition, and cooling rate (Reiners et al., 2018; Fig. S5 in the Supplemental Material). Because we target the signal from Namche Barwa, inferred to be the most rapidly exhuming part of the sediments' source area, we employ the minimum-age approach (Galbraith, 2005) to determine the youngest detrital age populations (see the Supplemental Material for details). Sample preparation and analytical methods are reported in the Supplemental Material; single-grain ages are in Tables S2–S4 and Figures S1–S3. All ages are interpreted as cooling ages, as justified in the Supplemental Material.

A plot of the minimum ages of our samples together with literature data as a function of depositional age (Fig. 2) shows two distinct groups: for all three thermochronometers, samples with depositional ages >7.5 Ma have lag times (Bernet et al., 2001) that are >5 m.y., whereas samples with depositional ages ≤7 Ma show short lag times (~2–3 m.y.). The latter group also shows several age inversions, where the system with lower closure temperature (ZFT) has minimum ages older than those for higher-closure-temperature systems (MAr, RUPb). Such inversions are expected at high exhumation rates in some circumstances (Reiners et al., 2018); alternatively, some of these minimum ages may be unreliable for analytical reasons (i.e., poor counting statistics for grains with low daughter-product abundance; see discussion in the Supplemental Material). We discriminate between (1) "internally consistent" samples, yielding ages ordered with respect to system closure temperatures within a sample and increasing monotonically with depositional age for the same system between samples, and (2) inconsistent samples, which do not meet these criteria.

QUANTIFYING NAMCHE BARWA EXHUMATION

The slope of the lag-time trend indicates whether exhumation rates were steady, increasing, or decreasing through time (Bernet et al., 2001). We used a Bayesian approach (Glotzbach et al., 2011) to fit single- and multi-tier linear regressions to the lag times of internally consistent minimum ages (see the Supplemental Material). The results (Fig. S4) indicate increasing exhumation before ca. 7 Ma, followed by rapid steady exhumation between ca. 7 Ma and 0.5–2.0 Ma, and probable further acceleration since 0.5–2.0 Ma indicated by the youngest two to three samples. However, the onset of rapid exhumation would precede the arrival of young grains in the sedimentary record because of (1) the time required to exhume rocks from the thermochronologic closure depth to the surface, and (2) the time required to re-equilibrate the crustal thermal structure.

To better constrain the exhumation history, we used a one-dimensional version of the thermo-kinematic code Pecube (Braun et al., 2012) to predict a time series of cooling ages
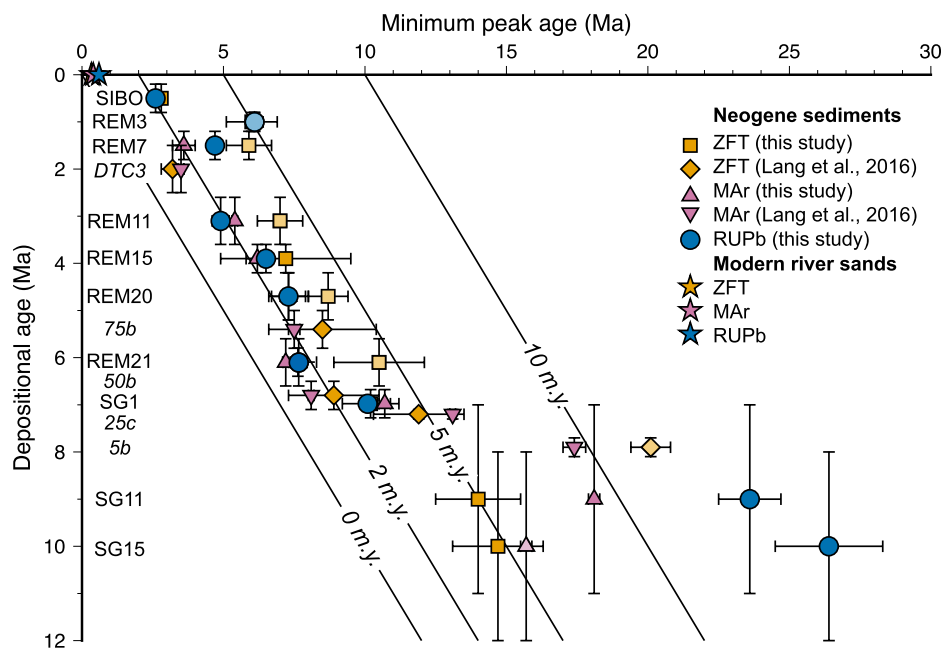
Figure 2. Minimum peak ages for new and previously published detrital thermochronology data from the easternmost Himalaya, as a function of depositional age. Horizontal and vertical error bars represent standard error on minimum age and depositional age intervals, respectively. Selected lag-time contours (in m.y.) are shown as black lines. Data in lighter shade are internally inconsistent and not used in the preferred modeling runs. ZFT—zircon fission track; MAr—muscovite $^{40}Ar/^{39}Ar$; RUPb—rutile U-Pb. Sample numbers (Table S1 [see footnote 1]) indicate section (REM—Remi; SG—Siang; see Fig. 1B). Lang et al. (2016) samples (sample numbers in italics) are from Siji section (see Fig. 1B). Modern river-sand data are from Stewart et al. (2008) and Enkelmann et al. (2011) (ZFT); Bracciali et al. (2016) (ZFT, RUPb); and Lang et al. (2016) and Gemignani et al. (2018) (MAr).

resulting from step changes in exhumation rates, accounting for the effect of heat advection during exhumation. Comparison with the detrital thermochronology data is achieved through neighborhood-algorithm inversion; the model inverts for the exhumation rates and the timing of rate changes (Braun et al., 2012). Inversions use either the full data set or only the internally consistent ages, and incorporate uncertainties in both minimum-peak ages and depositional ages. Two-stage and three-stage exhumation scenarios were tested. A full description of the procedure and the different inversions is provided in the Supplemental Material.

Our best-fit inversion uses the internally consistent data set and implies a three-stage exhumation history for the Namche Barwa massif, with an early (8.2 ± 1.8 Ma) onset of rapid exhumation and a late (1.3 ± 0.8 Ma) acceleration (Fig. 3). Initial, intermediate, and final exhumation rates are 0.9 ± 0.4, 4.0 ± 2.0, and 8.6 ± 1.0 km/m.y., respectively. The onset of rapid exhumation at ca. 8 Ma is consistent with metamorphic pressure-temperature-time (*P-T-t*) paths from the Namche Barwa massif (Palin et al., 2015). Predicted exhumation rates agree with estimates from bedrock thermochronology (Seward and Burg, 2008; Zeitler et al., 2014; Bracciali et al., 2016), including those indicating a recent (<1 Ma) acceleration (King et al., 2016). The total amount of exhumation since ca.

8 Ma predicted by our model is 42 ± 26 km, 1–4 times the ~15–20 km of exhumation since ca. 8 Ma inferred from *P-T-t* data (Fig. S8).

DISCUSSION

Exhumation rates in Namche Barwa prior to ca. 8 Ma are comparable with those elsewhere in the Greater Himalaya during the Neogene (e.g., Thiede and Ehlers, 2013), suggesting similar tectonic processes. *P-T-t* data (Fig. S8) suggest significant exhumation prior to ca. 8 Ma, captured by the initial phase of our model. In contrast, the clear evidence for accelerating exhumation at ca. 8 Ma and <2–3 m.y. lag times for all systems since that time, which we link to focused rapid exhumation in Namche Barwa, distinguish this easternmost detrital thermochronology record from those elsewhere in the Himalaya (e.g., Szulc et al., 2006; Chirouze et al., 2013). Our finding of sustained rapid exhumation since the late Miocene is consistent with previous work (Lang et al., 2016). However, inclusion of a high-temperature thermochronometer (RUPb) coupled with Pecube inversions allows us to reconstruct a more detailed three-stage exhumation history, reconciling previous apparently contrasting interpretations that emphasized either the earlier (ca. 8 Ma; Booth et al., 2009; Zeitler et al., 2014) or later (<2 Ma; Wang et al., 2014; King et al., 2016) time of exhumation-rate change.

The onset of rapid exhumation at ca. 8 Ma is consistent with the scenario envisaged by Zeitler et al. (2014). The discrepancy between the amount of post–ca. 8 Ma exhumation predicted by our data and that inferred from *P-T-t* data, for all but our lowest predicted exhumation rates, implies lateral inflow of mid-crustal material, consistent with the tectonic-aneurysm model (Zeitler et al., 2001a, 2001b; Koons et al., 2013). Thus, efficient coupling between crustal rock advection and surface erosion may have initiated at ca. 8 Ma, requiring the existence of a large throughgoing river system at that time. Whereas sedimentary provenance data record a drainage connection between the Yarlung-Tsangpo and the Brahmaputra since the early Miocene (ca. 18 Ma; Lang and Huntington, 2014; Bracciali et al., 2015; Blum et al., 2018), it is unclear when the drainage pathway through the Namche Barwa massif via the Siang was established (Govin et al., 2018).

The trigger for rapid exhumation in Namche Barwa remains debated. It could have been initiated by indenter-corner dynamics (Burg et al., 1998; Bendick and Ehlers, 2014), with coupling between river incision and rapid exhumation developing subsequently, or it could have resulted from capture of the Yarlung-Tsangpo by the Siang shortly before ca. 8 Ma. The latter scenario is consistent with river-incision patterns upstream of Namche Barwa, which have been interpreted to record a wave of incision migrating upstream since ca. 10 Ma (Schmidt et al., 2015). However, that scenario requires prior Yarlung-Tsangpo drainage to the foreland via another, as yet unconstrained, pathway, a prediction that may be tested by provenance analysis of proximal foreland sediment records from candidate fossil trans-orogenic river systems.

Quaternary uplift of the Namche Barwa massif has been inferred from a thick wedge of post–2.6 Ma alluvium preserved immediately upstream (Wang et al., 2014; Fig. 4). This ponded sediment implies that rock uplift temporarily outpaced river incision, steepening the Siang River profile downstream. Quaternary capture of the Parlung River by the Yarlung-Tsangpo-Siang, as suggested by thermochronology (Seward and Burg, 2008; Zeitler et al., 2014) and provenance data (Lang and Huntington, 2014; Govin et al., 2018), would have increased erosional power in the gorge downstream of the capture point. In turn, this may have strengthened the feedback loop and triggered enhanced uplift and exhumation of Namche Barwa. River profiles provide insight into this possibility. The modern Yarlung-Tsangpo-Siang and Indus River profiles differ (Korup et al., 2010; Fig. 4), even though both flow through rapidly exhuming syntaxial massifs (Burbank et al., 1996; Zeitler et al., 2001b; Finnegan et al., 2008; Korup et al., 2010). The inferred pre-Quaternary profile of the Yarlung-Tsangpo-Siang resembles the modern Indus profile, with a more subdued knickzone across
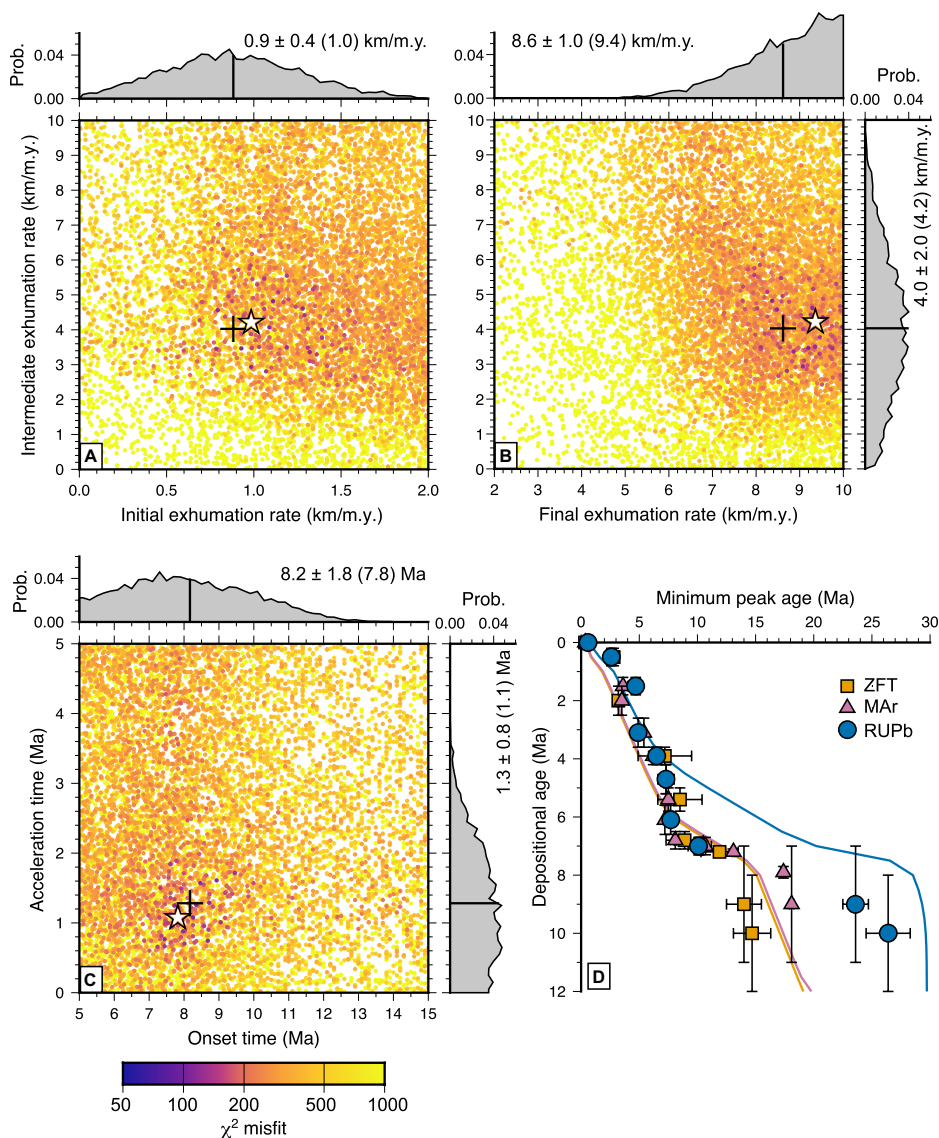
Figure 3. Result of preferred three-stage thermo-kinematic model inversion. (A–C) Individual forward-model results (dots colored according to misfit) and posterior probability-density functions (PDFs) of the parameter values (Prob.—probability). (A) Initial exhumation rate versus intermediate exhumation rate. (B) Final exhumation rate versus intermediate exhumation rate. (C) Onset time versus acceleration time. Crosses in scatterplots and thick lines in PDFs indicate most likely parameter values, indicated next to PDF with 1σ uncertainty; stars indicate best-fit model parameters (in parentheses next to PDF). (D) Fit of best-fit model (colored lines; orange—zircon fission track [ZFT]; purple—muscovite ⁴⁰Ar/³⁹Ar [MAr]; blue—rutile U-Pb [RUPb]) to data (colored symbols with error bars, as in Fig. 2).

Namche Barwa and a morphologic plateau edge located farther upstream. Modeling of river incision (Koons et al., 2013) shows that the differences in modern river profiles can be induced by differing rock-uplift rates in the syntaxial massifs of ~5 and ~10 mm/yr (Fig. 4), consistent with the recent acceleration our data imply.

CONCLUSIONS

Our new data and modeling reveal a three-stage exhumation history for Namche Barwa, reconciling previous studies focusing on either an early or a late onset of rapid exhumation. Our results suggest that coupling between crustal rock advection and surface erosion initiated in the late

Miocene and strengthened during the Quaternary. They suggest a potential role for river capture events in initiating and strengthening tectonic-erosion couplings in a tectonic aneurysm.

REFERENCES CITED

Bendick, R., and Ehlers, T.A., 2014, Extreme localized exhumation at syntaxes initiated by subduction geometry: Geophysical Research Letters, v. 41, p. 5861–5867, https://doi.org/10.1002/2014GL061026.

Bernet, M., Zattin, M., Garver, J.I., Brandon, M.T., and Vance, J.A., 2001, Steady-state exhumation of the European Alps: Geology, v. 29, p. 35–38, https://doi.org/10.1130/0091-7613(2001)029<0035:SSEOTE>2.0.CO;2.

Blum, M., Rogers, K., Gleason, J., Najman, Y., Cruz, J., and Fox, L., 2018, Allogenic and autogenic signals in the stratigraphic record of the deep-sea Bengal Fan: Scientific Reports, v. 8, 7973, https://doi.org/10.1038/s41598-018-25819-5.

Booth, A.L., Chamberlain, C.P., Kidd, W.S.F., and Zeitler, P.K., 2009, Constraints on the metamorphic evolution of the eastern Himalayan syntaxis from geochronologic and petrologic studies of Namche Barwa: Geological Society of America Bulletin, v. 121, p. 385–407, https://doi.org/10.1130/B26041.1.

Bracciali, L., Najman, Y., Parrish, R.R., Akhter, S.H., and Millar, I., 2015, The Brahmaputra tale of tectonics and erosion: Early Miocene river capture in the Eastern Himalaya: Earth and Planetary Science Letters, v. 415, p. 25–37, https://doi.org/10.1016/j.epsl.2015.01.022.

Bracciali, L., Parrish, R.R., Najman, Y., Smye, A., Carter, A., and Wijbrans, J.R., 2016, Plio-Pleistocene exhumation of the eastern Himalayan syntaxis and its domal 'pop-up': Earth-Science Reviews, v. 160, p. 350–385, https://doi.org/10.1016/j.earscirev.2016.07.010.

Braun, J., van der Beek, P., Valla, P., Robert, X., Herman, F., Glotzbach, C., Pedersen, V., Perry, C., Simon-Labric, T., and Prigent, C., 2012, Quantifying rates of landscape evolution and tectonic processes by thermochronology and numerical modeling of crustal heat transport using PECUBE: Tectonophysics, v. 524–525, p. 1–28, https://doi.org/10.1016/j.tecto.2011.12.035.

Burbank, D.W., Leland, J., Fielding, E., Anderson, R.S., Brozovic, N., Reid, M.R., and Duncan, C., 1996, Bedrock incision, rock uplift and threshold hillslopes in the northwestern Himalayas: Nature, v. 379, p. 505–510, https://doi.org/10.1038/379505a0.

Burg, J.-P., Nievergelt, P., Oberli, F., Seward, D., Davy, P., Maurin, J.-C., Diao, Z., and Meier, M., 1998, The Namche Barwa syntaxis: Evidence for exhumation related to compressional crustal folding: Journal of Asian Earth Sciences, v. 16, p. 239–252, https://doi.org/10.1016/S0743-9547(98)00002-6.

Chirouze, F., Huyghe, P., van der Beek, P., Chauvel, C., Chakraborty, T., Dupont-Nivet, G., and Bernet, M., 2013, Tectonics, exhumation, and drainage evolution of the eastern Himalaya since 13 Ma from detrital geochemistry and thermochronology, Kameng River Section, Arunachal Pradesh: Geological Society of America Bulletin, v. 125, p. 523–538, https://doi.org/10.1130/B30697.1.

Enkelmann, E., Ehlers, T.A., Zeitler, P.K., and Hallet, B., 2011, Denudation of the Namche Barwa antiform, eastern Himalaya: Earth and Planetary Science Letters, v. 307, p. 323–333, https://doi.org/10.1016/j.epsl.2011.05.004.

Finnegan, N.J., Hallet, B., Montgomery, D.R., Zeitler, P.K., Stone, J.O., Anders, A.M., and Liu, Y., 2008, Coupling of rock uplift and river incision in the Namche Barwa–Gyala Peri massif, Tibet: Geological Society of America Bulletin, v. 120, p. 142–155, https://doi.org/10.1130/B26224.1.

Galbraith, R.F., 2005, Statistics for Fission Track Analysis: Boca Raton, Florida, Chap-
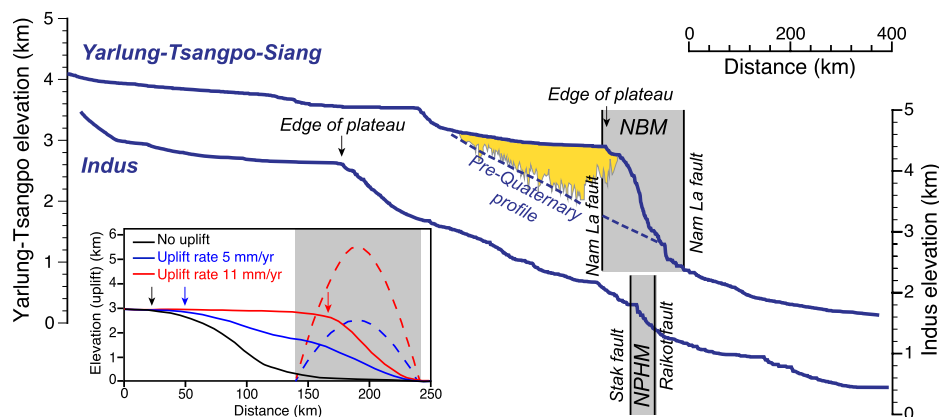
Figure 4. Indus and Yarlung-Tsangpo-Siang River profiles. Zones of rapid uplift and exhumation in Nanga Parbat–Haramosh (NPHM) and Namche Barwa (NBM) massifs are shown as gray boxes with bounding faults in black. The edge of the morphologic Tibetan Plateau is indicated with a vertical arrow. Thickness of Quaternary alluvial sediments (yellow) upstream of Namche Barwa is from Wang et al. (2014); inferred pre-Quaternary profile is indicated with dashed line. Inset (modified from Koons et al., 2013) shows modeled river profile (solid line) and rock uplift (dashed) after 0.5 m.y. for river incising a 3-km-high plateau bounded by a zone of anticlinal uplift (gray), for maximum uplift rates of 0 (black), 5 (blue), and 11 (red) mm/yr. Arrows indicate morphologic edge of the plateau.

man and Hall/CRC, 218 p., https://doi.org/10.1201/9781420034929.

Gemignani, L., van der Beek, P.A., Braun, J., Najman, Y., Bernet, M., Garzanti, E., and Wijbrans, J.R., 2018, Downstream evolution of the thermochronologic age signal in the Brahmaputra catchment (eastern Himalaya): Implications for the detrital record of erosion: Earth and Planetary Science Letters, v. 499, p. 48–61, https://doi.org/10.1016/j.epsl.2018.07.019.

Glotzbach, C., van der Beek, P.A., and Spiegel, C., 2011, Episodic exhumation and relief growth in the Mont Blanc massif, Western Alps from numerical modelling of thermochronology data: Earth and Planetary Science Letters, v. 304, p. 417–430, https://doi.org/10.1016/j.epsl.2011.02.020.

Govin, G., Najman, Y., Dupont-Nivet, G., Millar, I., van der Beek, P., Huyghe, P., O'Sullivan, P., Mark, C., and Vögeli, N., 2018, The tectonics and paleo-drainage of the easternmost Himalaya (Arunachal Pradesh, India) recorded in the Siwalik rocks of the foreland basin: American Journal of Science, v. 318, p. 764–798, https://doi.org/10.2475/07.2018.02.

King, G.E., Herman, F., and Guralnik, B., 2016, Northward migration of the eastern Himalayan syntaxis revealed by OSL thermochronometry: Science, v. 353, p. 800–804, https://doi.org/10.1126/science.aaf2637.

Koons, P.O., Zeitler, P.K., and Hallet, B., 2013, Tectonic aneurysms and mountain building, in Owen, L.A., ed., Treatise on Geomorphology, Volume 5: Tectonic Geomorphology: London, Academic Press, p. 318–349, https://doi.org/10.1016/B978-0-12-374739-6.00094-4.

Korup, O., Montgomery, D.R., and Hewitt, K., 2010, Glacier and landslide feedbacks to topographic relief in the Himalayan syntaxes: Proceedings of the National Academy of Sciences of the United States of America, v. 107, p. 5317–5322, https://doi.org/10.1073/pnas.0907531107.

Lang, K.A., and Huntington, K.W., 2014, Antecedence of the Yarlung-Siang-Brahmaputra River, eastern Himalaya: Earth and Planetary Science Letters, v. 397, p. 145–158, https://doi.org/10.1016/j.epsl.2014.04.026.

Lang, K.A., Huntington, K.W., Burmester, R., and Housen, B., 2016, Rapid exhumation of the eastern Himalayan syntaxis since the late Miocene: Geological Society of America Bulletin, v. 128, p. 1403–1422, https://doi.org/10.1130/B31419.1.

Najman, Y., Mark, C., Barfod, D.N., Carter, A., Parrish, R., Chew, D., and Gemignani, L., 2019, Spatial and temporal trends in exhumation of the Eastern Himalaya and syntaxis as determined from a multitechnique detrital thermochronological study of the Bengal Fan: Geological Society of America Bulletin, v. 131, p. 1607–1622, https://doi.org/10.1130/B35031.1.

Palin, R.M., Searle, M.P., St-Onge, M.R., Waters, D.J., Roberts, N.M.W., Horstwood, M.S.A., Parrish, R.R., and Weller, O.M., 2015, Two-stage cooling history of pelitic and semi-pelitic mylonite (sensu lato) from the Dongjiu-Milin shear zone, northwest flank of the eastern Himalayan syntaxis: Gondwana Research, v. 28, p. 509–530, https://doi.org/10.1016/j.gr.2014.07.009.

Reiners, P.W., Carlson, R.W., Renne, P.R., Cooper, K.M., Granger, D.E., McLean, N.M., and Schoene, B., 2018, Geochronology and Thermo-

chronology: Chichester, UK, John Wiley & Sons, 445 p., https://doi.org/10.1002/9781118455876.

Schmidt, J.L., Zeitler, P.K., Pazzaglia, F.J., Tremblay, M.M., Shuster, D.L., and Fox, M., 2015, Knickpoint evolution on the Yarlung river: Evidence for late Cenozoic uplift of the southeastern Tibetan plateau margin: Earth and Planetary Science Letters, v. 430, p. 448–457, https://doi.org/10.1016/j.epsl.2015.08.041.

Seward, D., and Burg, J.-P., 2008, Growth of the Namche Barwa Syntaxis and associated evolution of the Tsangpo Gorge: Constraints from structural and thermochronological data: Tectonophysics, v. 451, p. 282–289, https://doi.org/10.1016/j.tecto.2007.11.057.

Stewart, R.J., Hallet, B., Zeitler, P.K., Malloy, M.A., Allen, C.M., and Trippett, D., 2008, Brahmaputra sediment flux dominated by highly localized rapid erosion from the easternmost Himalaya: Geology, v. 36, p. 711–739, https://doi.org/10.1130/G24890A.1.

Szulc, A.G., et al., 2006, Tectonic evolution of the Himalaya constrained by detrital ^{40}Ar-^{39}Ar, Sm-Nd and petrographic data from the Siwalik foreland basin succession, SW Nepal: Basin Research, v. 18, p. 375–391, https://doi.org/10.1111/j.1365-2117.2006.00307.x.

Thiede, R.C., and Ehlers, T.A., 2013, Large spatial and temporal variations in Himalayan denudation: Earth and Planetary Science Letters, v. 371–372, p. 278–293, https://doi.org/10.1016/j.epsl.2013.03.004.

Wang, P., Scherler, D., Liu-Zeng, J., Mey, J., Avouac, J.P., Zhang, Y., and Shi, D., 2014, Tectonic control of Yarlung Tsangpo Gorge revealed by a buried canyon in Southern Tibet: Science, v. 346, p. 978–981, https://doi.org/10.1126/science.1259041.

Whipp, D.M., Jr., Beaumont, C., and Braun, J., 2014, Feeding the "aneurysm": Orogen-parallel mass transport into Nanga Parbat and the western Himalayan syntaxis: Journal of Geophysical Research: Solid Earth, v. 119, p. 5077–5096, https://doi.org/10.1002/2013JB010929.

Zeitler, P.K., et al., 2001a, Crustal reworking at Nanga Parbat, Pakistan: Metamorphic consequences of thermal-mechanical coupling facilitated by erosion: Tectonics, v. 20, p. 712–728, https://doi.org/10.1029/2000TC001243.

Zeitler, P.K., et al., 2001b, Erosion, Himalayan geodynamics, and the geomorphology of metamorphism: GSA Today, v. 11, no. 1, p. 4–9, https://doi.org/10.1130/1052-5173(2001)011<0004:EHGATG>2.0.CO;2.

Zeitler, P.K., Meltzer, A.S., Brown, L., Kidd, W.S.F., Lim, C., and Enkelmann, E., 2014, Tectonics and topographic evolution of Namche Barwa and the easternmost Lhasa block, Tibet, in Nie, J., et al., eds., Toward an Improved Understanding of Uplift Mechanisms and the Elevation History of the Tibetan Plateau: Geological Society of America Special Papers, v. 507, p. 23–58, https://doi.org/10.1130/2014.2507(02).